JOURNAL OF Materials CHEMISTRY

Preparation, characterization and mechanistic features of zirconia films on bare and functionalized gold surfaces

M. Aslam, Sushama Pethkar, K. Bandyopadhyay, I. S. Mulla, S. R. Sainkar, A. B. Mandale and K. Vijayamohanan*

Physical and Materials Chemistry Division, National Chemical Laboratory, Pune 411008, India. E-mail: viji@ems.ncl.res.in; Fax: 91-020-5893044

Received 25th January 2000, Accepted 6th April 2000
Published on the Web 30th May 2000

Electrochemical synthesis of microcrystalline ZrO_2 at room temperature on bare and functionalized gold surfaces is reported to illustrate the biomimetic conditions of nucleation and growth. ZrO_2 films prepared on self-assembled monolayers (SAMs) of pentane-1,5-dithiol (PDT) on polycrystalline gold surfaces reveal a high degree of orientation and a distinct cleavage face, in contrast to monoclinic films, obtained on bare gold surfaces at room temperature. Cyclic voltammetry (CV), X-ray photoelectron spectroscopy (XPS), impedance measurement, current-transients, X-ray diffraction (XRD) and scanning electron microscopy (SEM) were used to follow the monolayer formation, Zr-attachment on the SAM-modified surface and subsequent difference in nucleation conditions of ZrO_2 formation. The role of SAMs in controlling the size and habit during crystallization of ZrO_2 is discussed in terms of a proposed reaction mechanism.

I. Introduction

The recent past has seen increasing interest in the utilization of functionalized interfaces for growing ceramic thin films at temperatures below 100 °C.[1–5] Dense and highly adherent polycrystalline films of oxides, hydroxides and sulfides have been prepared on plastic, glass and other substrates, from aqueous as well as non-aqueous solutions using ω-functionalized self-assembled monolayers as organic templates for controlled nucleation and growth.[1–7] Due to the structural as well as functional similarities of self-assembled monolayers to protein surfaces, this type of preparation strategy is sometimes known as biomimetic synthesis as the monolayers play an important role by providing suitable functionalities necessary to initiate growth of the inorganic layers. For example, several studies have recently shown that by manipulation of surface energy through monolayer formation, nanophase morphology, crystal growth habit, orientation and even chirality can be controlled in both aqueous and non-aqueous media.[1–8]

Self-assembled monolayer (SAM) formation provides one effective approach for modifying a few selected substrate surfaces with a wide range of surface functionalities. One of the goals of SAM formation is to study the self-organization of various metal, semiconductor and insulator clusters on the SAMs with suitably tailored functionalities, so that active and passive components in microelectronic circuits can be made at low temperature using patterning of surfaces. The effective utilization of functionalized interfaces of SAMs for solid state and biomimetic synthesis is an active area of research, as elucidated by the multilayer formation of zirconium phosphonate and sequentially adsorbed copper ions on dithiol.[9,10]

In this work, we compare the electrochemical preparation of crystalline zirconia thin films at room temperature on bare and SAM-covered gold surfaces to elucidate the differences between the mechanisms of ZrO_2 formation. The formation of ceramic materials on SAM surfaces, especially on thiol moieties, will be interesting and extremely important from a biomineralization point of view. If the linkage between the terminal –SH of the SAM and the Zr^{4+} species is weak, the monolayer will collapse laterally during the electrochemical formation of zirconia. On the other hand, if there is a reasonably strong interaction between the terminal –SH and ZrO_2 tetramer,[11] in comparison with insignificant lateral interaction, the ZrO_2 molecules may not move to form long coherent islands. We have found that the chemical linking of Zr^{4+} onto SAMs of pentane-1,5-dithiol has a profound effect on the crystal habit and size compared to the ZrO_2 formed electrochemically on a bare gold surface. As the preparation of thin films of zirconia will be especially useful for a variety of applications such as fuel cells, oxygen sensors, inorganic membranes for gas separations, optical coatings *etc.*, this novel method is expected to influence many such applications. In addition, the present method also implies the possibility of preparing fully stabilized (cubic) or partially stabilized (tetragonal and cubic) zirconia on functionalized surfaces at lower temperatures by using various additives in the electrolyte.

II. Experimental

The gold substrates for these experiments were prepared by high vacuum (pressure better than 10^{-6} Torr) deposition of 2000 Å gold (purity 99.99%) on a conventionally cleaned glass slide with a Cr-buffer layer (50 Å) using the procedure described previously.[12] Zirconyl chloride octahydrate (99.9%) and pentane-1,5-dithiol obtained from Aldrich were used as received. In all the experiments deionized water from a Milli-Q system was used. First, a SAM of the dithiol was formed on the gold film by dipping it in 1 mM ethanolic solution for 24 hours following established methods to obtain the equilibrium organization.[13,14] In the second step, the SAM-covered gold substrate was introduced in a 5 mM aqueous zirconyl oxychloride solution (pH ≅ 3.5) at ambient temperature for 24 hours to ensure complete attachment of Zr^{4+} ions to the ω-terminal groups of the SAMs. The treated substrate was then washed copiously with de-ionized water and dried under a flow of argon gas. Variation of the immersion time over 2–24 h as well as the concentration of the solution in the millimolar range produced identical results. In the final step, cyclic voltammetry was performed using the samples obtained from the second step as the working electrode, a large platinum flag as the counterelectrode and a saturated calomel (SCE) as the reference electrode in 1 M aqueous KCl solution. The potential was cycled between −1.2 and +0.8 V *vs.* SCE at a scan rate of

DOI: 10.1039/b000681p

200 mV s^{-1} as per the conditions reported earlier for the preparation of ZrO_2 films.[15,16] To confirm Zr attachment on the SAM surface, cyclic voltammetry was also performed on the bare and SAM-covered gold substrates respectively, as working electrodes in a mixture of 1 M KCl and 5 mM $ZrOCl_2$ solution. After performing at least ten such cycles the samples were removed and washed with a gentle flow of de-ionized water and dried under Ar prior to characterization.

Cyclic voltammetry was carried out with a computer-interfaced PAR 283 potentiostat/galvanostat as described above using bare as well as SAM-covered Au as the working electrode under normal atmosphere. Impedance measurements were performed with a PAR 283 potentiostat/galvanostat and a PAR 5012 lock-in amplifier interfaced with a computer, in a solution containing 5 mM of the redox-active probe, $Fe(CN)_6^{3-/4-}$. Impedance measurements always used a 5 mV rms perturbation at the formal potential of the redox couple and readings were taken at five discrete frequencies per decade. The analysis was carried out using the commercially available program EQUIVALENT CIRCUIT written by B.A. Boukamp (University of Twente) which determines the parameters of the assumed equivalent circuit by a weighted non-linear least-squares fit.

The XPS measurements were carried out using a VG Scientific ESCA 3 MK II spectrometer operated at a pressure of 10^{-9} Torr using a monochromatic Mg-Kα source ($h\nu = 1253.6$ eV). The alignment of the binding energy was done using the C 1s binding energy of 284.6 eV as a reference. The X-ray flux was kept deliberately low in order to reduce beam-induced damage (electron power 70 W). The deconvolution of overlapping peaks in the final, high resolution spectra was accomplished using a standard curve-fitting algorithm. The line shape of all peaks was assumed to be Gaussian. The X-ray diffraction analysis of the films was carried out at room temperature using a Philips 1730 X-ray diffractometer at 40 kV and 30 mA (1200 W) with filtered Cu-Kα line ($\lambda = 1.5404$ Å). Scanning electron microscopy (SEM) of the sample was conducted on a Leica Stereoscan S-440 model microscope, operated at 20 kV accelerating voltage and 25 pA current.

III. Results and discussion

III.1. X-Ray diffraction analysis

The XRD patterns of the dry as-deposited and annealed zirconia films, prepared potentiodynamically on SAM-covered and bare gold surfaces, are shown in Figs. 1 and 2 respectively. The XRD pattern (Fig. 1a) of the as-deposited (room temperature) sample on a SAM functionalized surface indicates a highly oriented monoclinic nature for the ZrO_2 film. More specifically, this data shows two major peaks (●) belonging to the (111) and (222) planes of zirconia, perhaps due to the strong (111) preferred orientation of the gold film induced by the hexagonal structure of the dithiol SAM. Annealing of the film at 100 °C (Fig. 1b) shows a marked decrease in intensity of all the zirconia peaks, whereas the intensities of the gold peaks (■) appear to increase. A further increase in annealing temperature to 200 °C (Fig. 1c) reveals that the ZrO_2 peaks are completely diminished, leaving the remaining gold peaks only. We believe that the SAM provides a strong periodic field for the orientation of zirconia nuclei and this order is lost when the monolayer is thermally decomposed. The crystallites may take a random orientation (rather than becoming amorphous) and the probable reason for the loss of reflection is due to the formation of amorphous ZrO_2 on the annealed surface. In contrast to Fig. 1a, the XRD pattern of ZrO_2 coated on a bare gold surface (Fig. 2a) shows relatively intense gold peaks along with zirconia peaks. The annealing of the film at 300 °C (Fig. 2b) shows a similar decrease in the intensity of zirconia peaks but no disappearance, unlike the case of the functionalized surface, indicating the influence of the thiol monolayer on crystallinity.

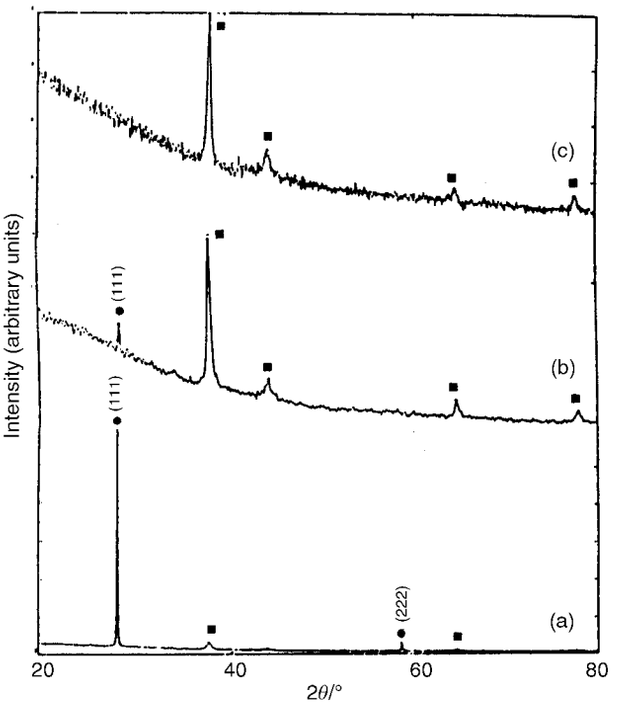

Fig. 1 XRD pattern of zirconia films on a PDT SAM coated gold surface by potentiodynamic cycling (a) at room temperature, (b) calcined at 100 °C, and (c) after annealing at 200 °C. The peaks corresponding to the underlying gold substrate are marked by (■) while those of zirconia are indicated by (●).

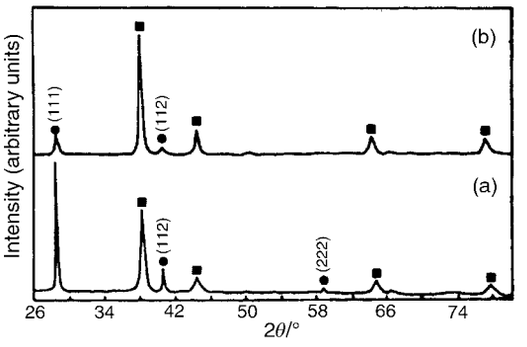

Fig. 2 XRD pattern of zirconia films prepared on a bare gold substrate (a) at room temperature and (b) annealed at 300 °C. Similar marks are given for zirconia and gold peaks as indicated above.

The change in crystallite size was calculated using the line broadening of the (111) peak with the aid of the Scherrer equation.[17] The crystallite size was found to be 40–50 nm for as-deposited samples in both the cases. Interestingly, the annealed samples show a decrease in particle size (20–30 nm) upon heating, in contrast to the amorphous to polycrystalline progression known in zirconia films.[18–20] It is unlikely to have undergone a transition from crystalline to amorphous by annealing and hence the disappearance of the preferred orientation indicates that the ordering of the SAM enables unique crystalline features during nucleation.

III.2. Cyclic voltammetry

A significant change in double layer capacitance as approximately estimated from fast scan voltammetry is a commonly used procedure to evaluate monolayer formation and quality.[21] Fig. 3 shows such a superimposed cyclic voltammogram taken

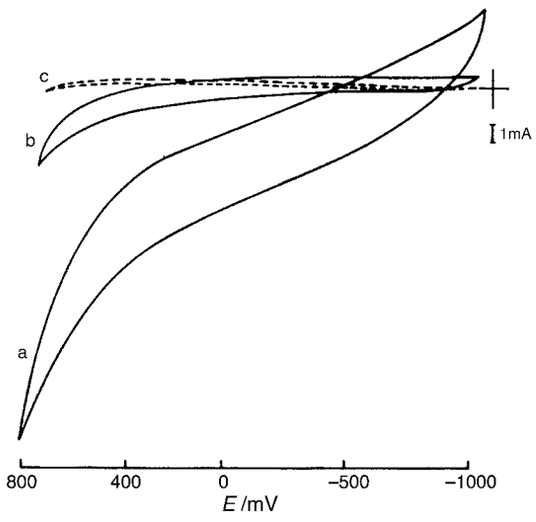

Fig. 3 Superimposed cyclic voltammogram in 1 M KCl (a) at a bare gold electrode, (b) at a gold electrode modified with a SAM of PDT, and (c) after attachment of Zr from 5 mM $ZrOCl_2$ on the SAM surface with a typical scan rate of 500 mV s^{-1}.

at 500 mV s^{-1} for a bare gold electrode, a gold electrode modified with dithiol and a gold electrode modified with dithiol after adsorption of Zr ions, all using 1 M aqueous KCl solution. The dithiol SAM formation is evident from the significant decrease of the nonfaradaic current (Fig. 3b, c). More importantly, the passivation of the surface is complete after Zr^{4+} attachment. An approximate calculation of the double layer capacitance from this data on the basis of reported surface roughness[22] yields 40 μF cm^{-2} for bare gold, whereas 5.5 and 2.1 μF cm^{-2} are obtained for the dithiol-modified electrode and the Zr-attached SAM surface, respectively. These values obtained for bare gold and SAM-covered gold are comparable to the respective values reported earlier and the change in capacitance corresponds to similar SAMs with 99% surface coverage.[23] As capacitance is determined by dielectric permittivity, the thickness of the adsorbed layer and the packing density of the adsorbed molecule, a further reduction after Zr attachment suggest that either the Zr species from the solution has increased the separation of charge between the electrode surface and plane of closest approach or decreased the polarizibility of the intervening medium.

In order to understand the difference in ZrO_2 film formation on bare and functionalized Au surfaces from Zr^{4+} ions in solution, cyclic voltammetry was also conducted in a 1 M KCl solution containing a 5 mM aqueous solution of zirconium oxychloride. Fig. 4 shows a representative superimposed cyclic voltammogram at 200 mV s^{-1} using gold-coated glass and SAM-functionalized gold-coated glass as working electrodes respectively. An irreversible reduction peak at −0.9 V *vs.* SCE is clearly seen in both the cases. The minor oxygen reduction peak observed for the bare electrode is absent on the SAM-covered gold electrode. The potential range for CV in this case is the same as that used for zirconia preparation. The type of cyclic voltammetric response remains unchanged even after ten continuous potential cycles. The double layer capacitance (14 μF cm^{-2} for bare gold and 5.6 μF cm^{-2} for the SAM funtionalized gold surface) observed using a 200 mV s^{-1} scan rate at the end (Fig. 5) suggests that the monolayer is intact even after the cathodic formation of ZrO_2. Gold-coated glass substrates kept for 12 hours in $ZrOCl_2$ solution, washed then immersed in KCl showed a response like Fig. 5a, without any significant change in double layer capacitance, indicating that there is no surface functionalization in the absence of a dithiol monolayer.

It is instructive to compare all the features present in Fig. 4 to the voltammetric response obtained for a Pt working electrode in a similar solution.[15] Although the Pt working electrode shows a reversible couple at $E_{1/2}$ of −0.49 V *vs.* SCE along with the same anodic and cathodic peak current, Au shows only an irreversible reduction at −0.9 V, irrespective of the presence of a monolayer. A comparison of the electrochemistry of $ZrOCl_2$ on Au and Pt electrodes indicates that the mechanisms of ZrO_2 formation are different on these two electrode surfaces. Zirconia formation by reduction is thought to occur *via* the following plausible scheme.[15]

$$ZrOCl_2 + e^- \rightleftharpoons ZrOCl + Cl^-$$

$$2ZrOCl + 2H_2O \rightleftharpoons 2ZrO_2 + 2HCl + H_2$$

However, the actual mechanism may be more complex for a number of reasons. First, $ZrOCl_2$ is not a simple molecule containing Zr–Cl bonds, it is a tetrameric hydrolysis product in which all bonds of Zr are to O (hydrolysis of water). Although Zr can exhibit the +3 oxidation state in compounds such as $ZrCl_3$, such compounds are completely unstable in water. In aqueous environments, Zr^{III} is instantaneously oxidised to Zr^{IV} and all Zr–Cl bonds are hydrolysed to form Zr–O bonds. The resulting hydrolysis products are only soluble in strong acids or strong base. Hence, the reaction scheme given above may not be possible for gold. An alternate explanation to realise the electrochemical activity for dissolved $ZrOCl_2$ which promotes ZrO_2 formation is that water molecules coordinated to Zr are being electrolysed to produce H_2 and more anionic oxygens.

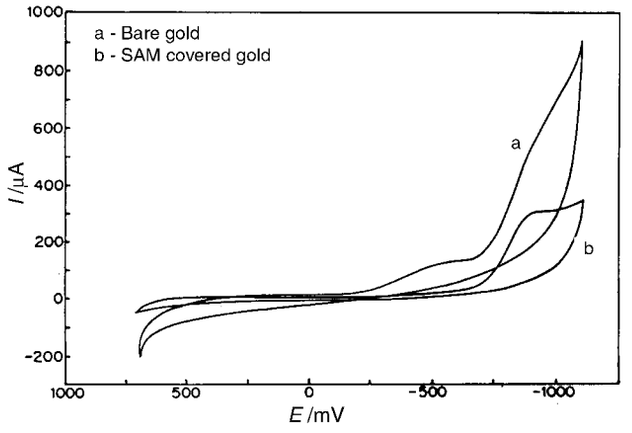

Fig. 4 Superimposed cyclic voltammogram in 1 M KCl and 5 mM zirconyl oxychloride aqueous solution (a) at a bare gold electrode, and (b) at a SAM functionalized gold electrode, with a typical scan rate of 200 mV s^{-1}.

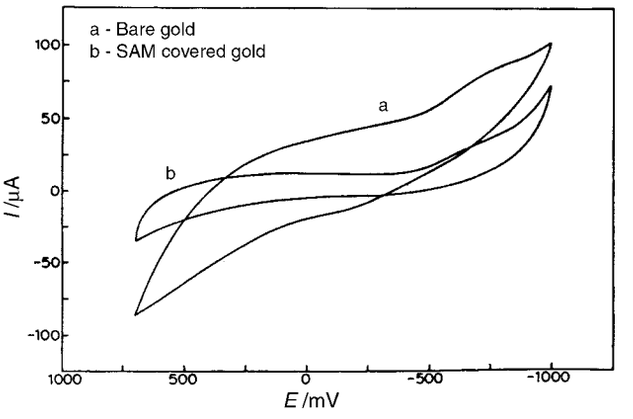

Fig. 5 Superimposed cyclic voltammogram in 1 M KCl (a) at a bare gold electrode, and (b) at a SAM functionalized gold electrode after subsequent adsorption of Zr ions from 5 mM $ZrOCl_2$ on both the surfaces, with a typical scan rate of 200 mV s^{-1}.

Such oxygens would be more active for polymerisation than the coordinated waters. The observed electrochemical potentials are in the right range to be consistent with such a scheme. Another factor could be that if electrolysis is creating pH gradients near the electrode surfaces, it can also stimulate the nucleation of ZrO_2 simply by changing the pH. The Zr species need not be a direct participant in the electrochemical reaction itself.

The decreased current values indicated in Fig. 4 for the dithiol-functionalized electrode can be understood either in terms of an increase in the ohmic resistance due to monolayer formation or merely a reduction in nucleation sites due to the partitioning of the available area. The SAM head groups might be expected to form a stable complex with dissolved zirconia species. The sulfate head group is known to be capable of displacing coordinated waters to form a stable complex. Since the –SH group terminating the alkane thiol group has a pK_a of about 9, a neutral –SH is present initially in the solution, which then reacts with tetrameric $ZrOCl_2$ to produce ZrO attached to the SAM surface, eliminating HCl. The short chains possibly avoid the problem of dithiol looping on the gold surface[24] providing free thiol on the surface to anchor the zirconium ions. The Zr attachment on the terminal functional group (–SH) rather than ZrO_2 formation on defects and pinhole regions is supported by the shape of the voltammograms, as there is no indication of spherical diffusion control.[25]

III.3. Current–time transients

Since the above cyclic voltammetric features (Fig. 4) suggest reductive ZrO_2 formation on both bare and functionalized Au surfaces with identical thermodynamic features (*i.e.* peak potential), current–time transients were used to study the difference in nucleation and growth aspects of the oxide film. Fig. 6 shows such a current–time response measured after stepping the potential from the open circuit value to −1.2 V *vs.* SCE, optimised primarily on the basis of voltammetry performed for the ZrO_2 formation. Although there is a pronounced maximum and a thousand-times decrease in the magnitude of the current for the case of the functionalized Au surface, the chronoamperometric data can be systematically analyzed after separating them into two regions (I and II in Fig. 6). The first region (*i.e.* time between 0 to t_o) corresponds to a sharp decrease in the current for both types of electrodes, whereas the second part of the curve shows distinct changes in nucleation

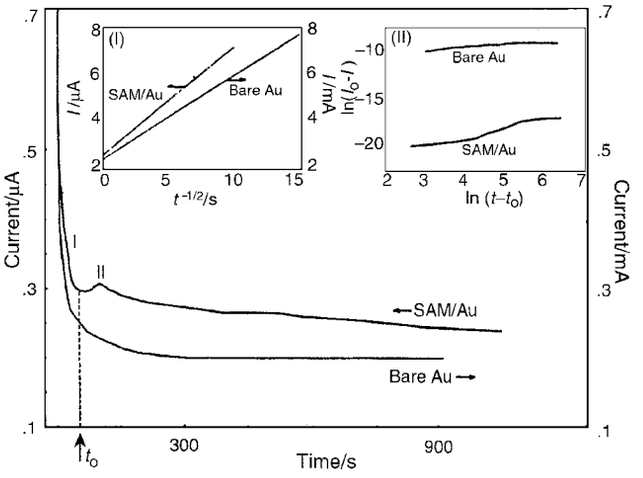

Fig. 6 Current–time transients for (I) the SAM functionalized electrode, and (II) the bare gold electrode, as indicated in the figure illustrating the behaviour observed at potential −1.2 V. The solution was 1 M aqueous KCl + 5 mM $ZrOCl_2$. At $t=0$ the potential was stepped from 0 to −1.2 V. The inset (I) indicates the plot of current *vs.* $t^{-1/2}$ ($t<t_o$) for the same composition and similar electrodes as described above and inset (II) describes the variation of $\ln(I-I_o)$ with respect to $\ln(t-t_o)$.

behaviour before reaching a final steady state current. For region ($t<t_o$), both the electrodes indicate a linear relationship between I and $t^{-1/2}$ (inset (I), Fig. 6) suggesting the mechanism of instantaneous nucleation corresponding to the growth of hemispherical nuclei kinetically controlled by planar or spherical diffusion. However, both the lines do not intersect the origin, perhaps due to deviation from an ideal Cottrell diffusion process. The increase in the slope for the SAM-covered gold substrate may be partly due to the difference in the charging behaviour (double layer capacitance change) and nucleation sites.

The second region ($t>t_o$), on the other hand, indicates a peak at the beginning for the SAM-covered gold substrate, whereas a slow decrease only is observed for bare gold, finally reaching a steady value. The peak is not sharp and could be associated with the reductive desorption of dithiol monolayers, as simple alkanethiols at Au(111) surfaces are known to desorb beyond −1.0 V in aqueous electrolytes.[26] The nucleation of ZrO_2 on the SAM surface can be delayed due to the linkage of Zr to the surface, while such a restriction is not present for the case of bare Au. The kinetics is also different as the nature of the process elucidates a linear relationship between $\ln(I_o-I)$ and $\ln(t-t_o)$ for the bare electrode, while a sigmoidal relation is observed for the SAM covered gold electrode (inset (II), Fig. 6). This indicates that the potentiostatic formation of ZrO_2 is driven by progressive nucleation which is controlled by planar diffusion in the case of bare Au and by spherical diffusion in the case of the SAM-covered Au electrode. The difference in kinetics is due to constraints, such as pinholes and structural defects offered by the SAM,[21] probably controls the rate of nucleation, leading to improved crystallinity of ZrO_2 film on SAM-covered gold.

III.4. Impedance measurements

Despite the ambiguities of model-dependant interpretation, impedance measurements based on the response of an electrochemical cell to a small amplitude alternating signal offers a convenient method to study monolayer[27] structure and integrity. For example, the process of monolayer formation and the subsequent covalent attachment of Zr^{4+} from aqueous solution to the SAM-covered surface was followed by impedance measurements in the presence of a redox active probe, $Fe(CN)_6^{4-/3-}$. In such systems, two distinct frequency regions can be separated in the presence of external redox agents like $Fe(CN)_6^{4-/3-}$ using the simplest Randles' equivalent circuit.[28] In the low-frequency region, mass transfer *via* diffusion has to be taken into account, whereas, the microarray behaviour of the pinholes within the passivating monolayer disturb the expected $\omega^{-1/2}$ dependence of Warburg impedance.[29] Defects or pinholes in the monolayer which are far apart from each other deviate from the semi infinite diffusion[12] and therefore spherical diffusion seems to be valid as overlap of diffusion layer is not achieved.[30]

A comparison of the complex impedance plots of bare gold (Fig. 7a) and monolayer-coated gold (Fig. 7b) shows the effect of adsorbed dithiol monolayer on the ac response of gold electrodes. The impedance spectrum for bare gold is not well defined (probably due to a fast electrode reaction) and the absence of a semicircle precludes any quantitative calculation. In sharp contrast, identification of a well defined semicircle for SAM-covered gold allowed us to calculate useful parameters, as it is known that at higher frequency the diameter of the semicircle corresponds to the R_{ct} of the monolayer coated electrode.[23] From the analysis of the spectrum in Fig. 7b, charge transfer resistance of 2109 Ω cm^2 is obtained[31] with a corresponding approximate electrode coverage of 99%.[32] This result shows that the dithiol has formed a highly compact and organised monolayer assembly on the Au surface to give a good platform for further adsorption of Zr^{4+} from solution.

Fig. 7c shows the complex impedance plot of the Au/SAM

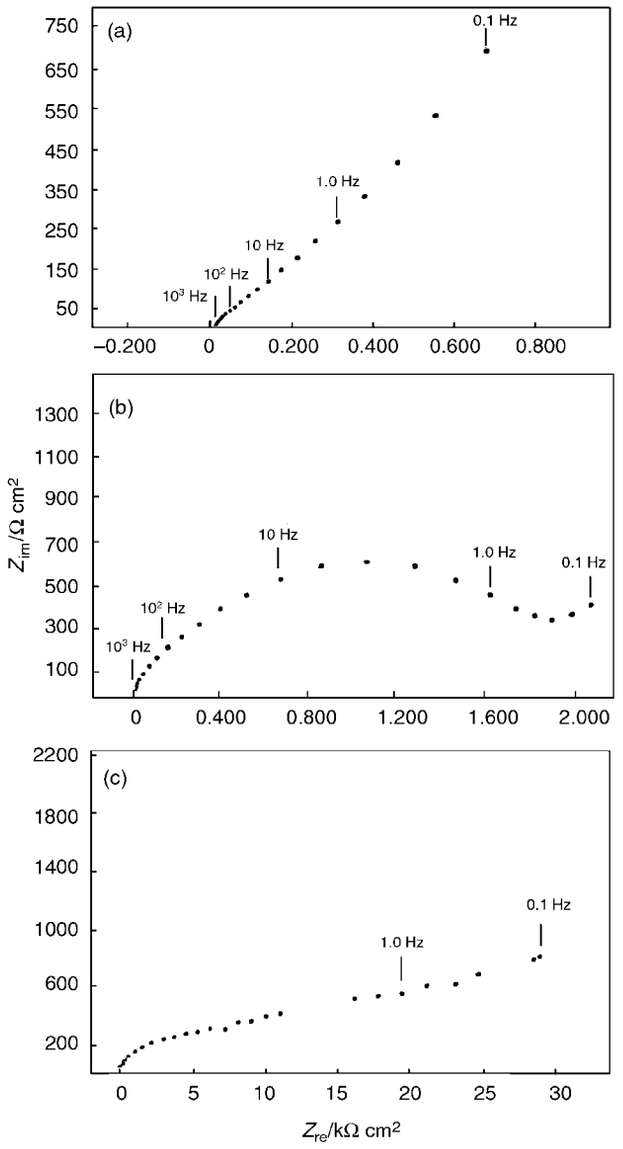

Fig. 7 Complex impedance plots at a dc bias of 0.22 V in 5 mM $K_3Fe(CN)_6$ + 5 mM $K_4Fe(CN)_6$ in 0.5 M aqueous KF solution for (a) a bare gold electrode, (b) a gold electrode with a pentane-1,5-dithiol SAM, and (c) a gold electrode with a pentane-1,5-dithiol SAM after Zr attachment on the SAM surface from a 5 mM solution of $ZrOCl_2$. Frequency range used is 100 kHz to 100 mHz with a 5 mM rms signal at five steps per decade.

electrode after adsorption of Zr^{4+} ion. Comparison with Fig. 7b indicates a more dispersed impedance response. The expected semicircle at higher frequencies is not well defined in this case, although an approximate semicircle fit gives a charge transfer value of 9277 $\Omega\,cm^2$. This drastic difference in impedance response of the two electrodes can be attributed to the attachment of Zr^{4+} from solution to the dithiol SAM covered surface which hinders the penetration of the redox probes. Since the monolayer acts as a barrier for ion permeation, adsorption of Zr ion on the SAM covered surface can make the electrode surface more passive and as a result of the electrostatic interactions, the permeation rate of ions becomes still lower.

III.5. X-Ray photoelectron spectroscopy

X-Ray photoelectron spectroscopic analysis of a Au substrate with dithiol monolayer formation and subsequent Zr attachment shows two peaks for sulfur core level spectra. The peak at lower binding energy after deconvolution shows two gaussian pairs consisting of spin–orbit components separated by a difference of 1.1 eV (Fig. 8a). The least-squares fit shows that there are two species of sulfur separated by 4.4 eV. The lower peak at *ca.*163 eV is in good agreement with that reported[33] earlier for chemisorbed thiol and dithiol monolayers on Au. The sulfur peak at *ca.* 167 eV is due to sulfate or sulfonic acid moieties[34] formed due to X-ray beam damage of the free thiols (*i.e.* not linked to Zr species) during the measurements.[35] The evidence of sulfur peak after the potential cycling demonstrates that the underlying dithiol monolayer is stable during the formation of ZrO_2 (Fig. 8b). Although the relative cross section of sulfur is very small, the binding energy values are particularly sensitive to the chemical environment of sulfur. The Zr 3d signal on a SAM covered gold surface before (Fig. 9a) and after (Fig. 9b) potentiodynamic cycling consists of a Zr $3d_{5/2}$ peak at *ca.* 182.4 eV and a Zr $3d_{3/2}$ peak at 185.6 eV, whereas the XPS data of a bare gold substrate dipped in a zirconyl oxychloride aqueous solution indicates no such peaks, revealing no Zr attachment on the bare gold surface before or after the cycling.

III.6. Scanning electron microscopy

Scanning electron microscopy performed on ZrO_2 obtained after potentiodynamic cycling on bare and functionalized Au surfaces shows interesting morphological features. First, distinct zirconia crystals possessing an average size of 5–10 μm can be seen on the SAM coated Au surface (Fig. 10a), suggesting the formation of uniform and sharp-edged crystals at room temperature. More significantly, the distinct separation between crystals (5–10 μm) due to Zr attachment on the SAM is missing for ZrO_2 formed on a bare gold substrate (Fig. 10c), where ZrO_2 particles distributed continuously with

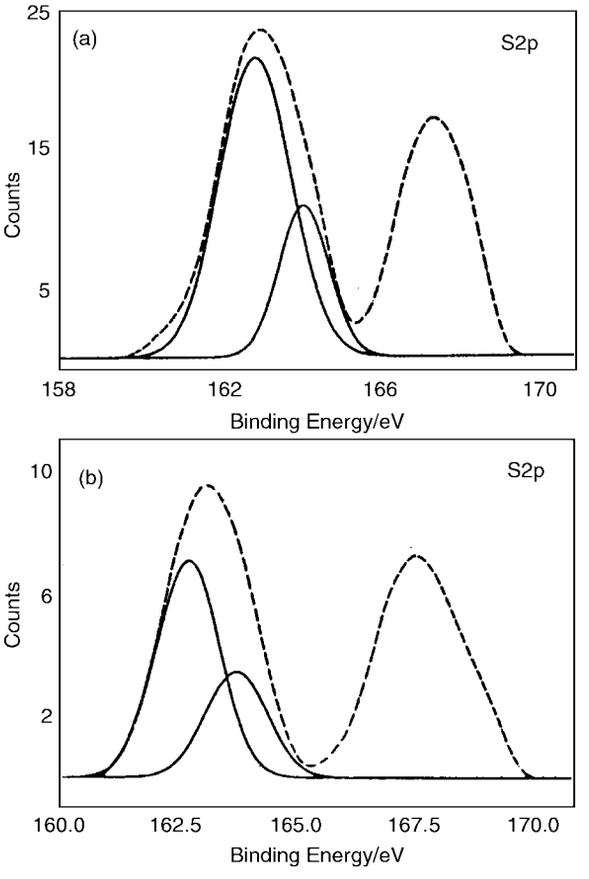

Fig. 8 X-Ray photoelectron spectra of (a) the S 2p core level after subsequent Zr adsorption on the self-assembled monolayer functionalized Au surface, and (b) the S 2p core level after potentiodynamic cycling between −1.2 and +0.8 V.

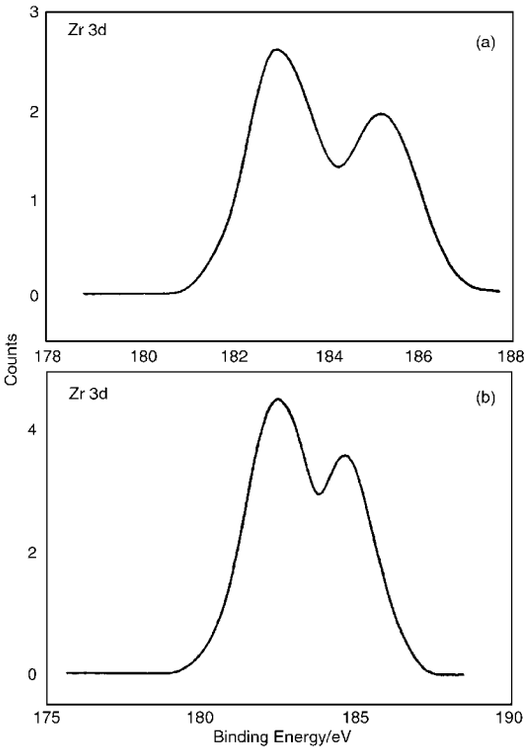

Fig. 9 X-Ray photoelectron spectrum of (a) the Zr 3d core level after subsequent Zr attachment on the SAM covered Au surface, and (b) the Zr 3d core level after potentiodynamic cycling between −1.2 and +0.8 V for the SAM functionalized Au surface.

an average interparticle distance of 5 μm suggest random nucleation. Even maintenance of −1.2 V for several hours (Fig. 10d) shows continuous growth of ZrO_2 films as compared to that for the functionalized interface. This type of variation in crystal habit exhibited by a given organic molecule is known to result from variations in the conditions under which the substance crystallised. This highlights the significance of SAMs in controlling the directional growth of the solid materials at the interface. This is specially significant for biomimetic processing of materials since several reports[36] have recently shown that the manipulation of the surface energies is possible through SAM formation to favour heterogeneous growth and nucleation.

All the above results indicate that microcrystalline zirconia with better topographic control can be grown at room temperature on SAM surfaces. The difference in nucleation and growth kinetics due to Zr attachment on the dithiol functionalized Au surface is primarily responsible for this, as evidenced in the current–time transients. The role of SAMs in this context is to be compared with the role of organic materials as manipulators of morphology, leaving an imprint of their original presence even after complete oxidation at high temperature.[37,38] We believe that this morphology difference is explained by the ability of SAMs to favour certain growth directions, as manifested from the relative microscopic evidence of crystals obtained in the absence of SAMs.

IV. Conclusions

The present study shows that the morphology of ceramic materials can be controlled using SAMs *via* Zr attachment on self-assembled monolayers of dithiol on a Au surface followed by a simple potentiodynamic cycling to give microcrystalline,

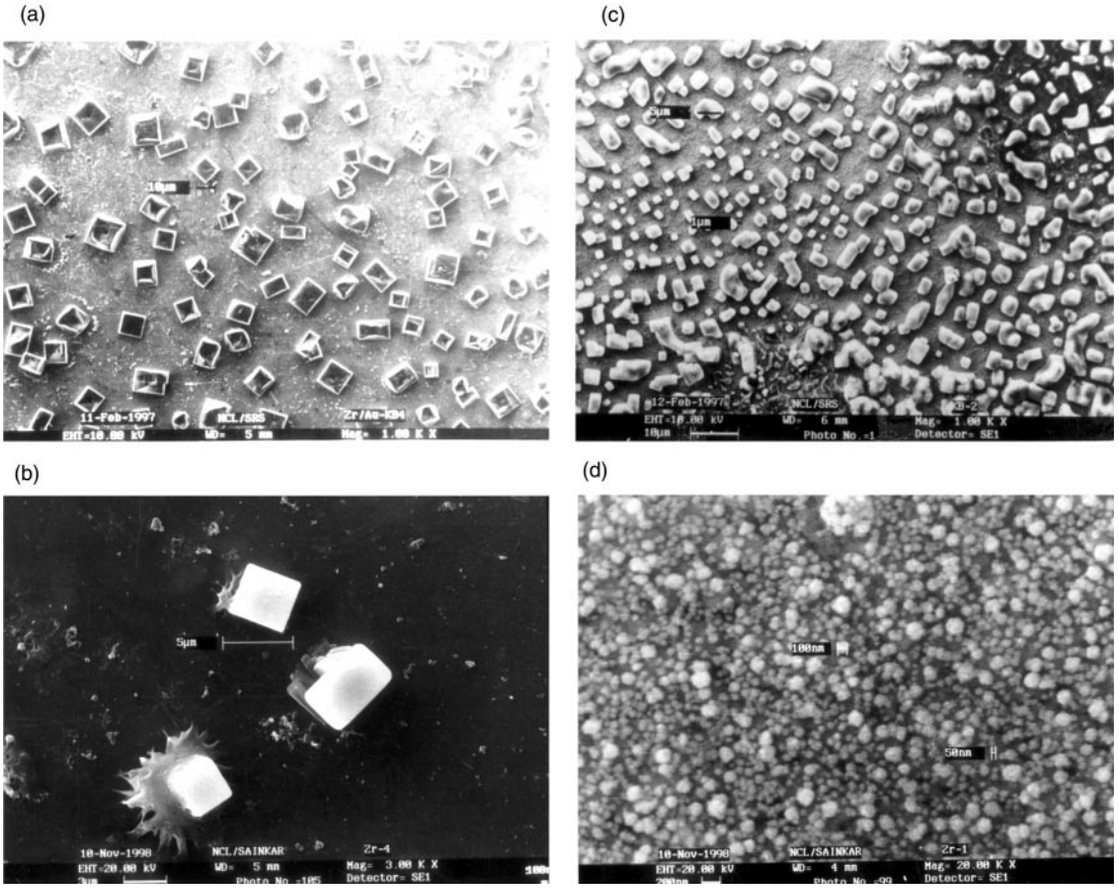

Fig. 10 Micrographs of microcrystalline zirconia on (a) a gold coated glass substrate derivatized with a SAM of pentane-1,5-dithiol, (b) a SAM functionalized gold surface with higher resolution, (c) a bare gold substrate, and (d) a bare gold substrate cycled for longer time. The samples were prepared by potentiodynamic cycling at a scan rate of 200 mV s^{-1} over a potential range of +0.7 to −1.1 V *vs.* SCE.

monoclinic ZrO_2 at room temperature. The results discussed here also suggest the possible use of self-assembled monolayers to effectively modify the morphology of ceramic thin films with promising applications in a wide range of fields including electrochemical sensors, electrocatalysis and ceramic coatings. A similar functionalization strategy could also be extended to prepare tetragonal or cubic zirconia at room temperature, with control of appropriate electrolyte composition.

Acknowledgements

M.A. thanks CSIR, New Delhi, for a Senior Research Fellowship. K.V. thanks the Department of Science and Technology, Government of India, for financial assistance. S.P. thanks CSIR, New Delhi, Government of India, for an RA fellowship. Discussions with Dr P. Ganguly, Physical Chemistry, National Chemical Laboratory, are gratefully acknowledged.

References

1 B. C. Bunker, P. C. Rieke, B. J. Tarasevich, A. A. Campbell, G. E. Fryxell, G. L. Graff, L. Song, J. Liu, J. W. Virden and G. L. McVay, *Science*, 1994, **264**, 48.
2 C. M. Bell, C. H. Yang and T. E. Mallouk, *Materials Chemistry (An Emerging Discipline)*, ed. L. V. Interrante, L. A. Casper and A. B. Ellise, 1995, p. 211.
3 M. Agarwal, M. R. De Guire and A. J. Heure, *J. Am. Ceram. Soc.*, 1997, **80**(12), 2967.
4 C. N. R. Rao, *J. Mater. Chem.*, 1999, **9**(1), 1.
5 H. Lee, L. J. Kepley, H. Hong, Sohail Akhtar and T. E. Mallouk, *J. Phys. Chem.*, 1988, **92**, 2597.
6 S. Mann, H. C. Nicholas, R. B. Frankel, D. A. Bazylinski and H. W. Jannasch, *Nature*, 1990, **343**, 258.
7 H. Shin, R. J. Collins, M. R. De Guire, A. H. Heure and C. N. Sukenik, *J. Mater. Res.*, 1995, **10**(3), 692.
8 P. C. Rieke, B. D. Marsh, L. L. Wood, B. J. Tarsevich, J. Liu, L. Song and G. E. Fryxell, *Langmuir*, 1995, **11**, 318.
9 B. L. Frey, D. G. Hanken and R. M. Corn, *Langmuir*, 1993, **9**, 1815.
10 M. Brust, P. M. Blass and A. J. Bard, *Langmuir*, 1997, **13**, 5602.
11 F. A. Cotton and G. Wilkinson, *Advanced Inorganic Chemistry*, 3rd edn., Wiley Eastern Ltd., 1972.
12 K. Bandyopadhyay, M. Sastry, V. Paul and K. Vijayamohanan, *Langmuir*, 1997, **13**, 866.
13 C. D. Bain, E. B. Troughton, Y. Tao, J. Evall, G. M. Whitesides and R. G. Nuzzo, *J. Am. Chem. Soc.*, 1989, **11**, 321.
14 C. D. Bain, J. Evall and G. M. Whitesides, *J. Am. Chem. Soc.*, 1989, **111**, 7155.
15 K. Bandyopadhyay, S. R. Sainkar and K. Vijayamohanan, *J. Am. Ceram. Soc.*, 1999, **82**(1), 622.
16 K. Bandyopadhyay and K. Vijayamohanan, *Langmuir*, 1998, **14**, 6924.
17 B. D. Cullity and C. Cohen, *Elements of X-ray diffraction*, Addison-Wesley Publishing Co. Inc., 1956.
18 T. Yao, T. Inui and A. Ariyoshi, *J. Am. Ceram. Soc.*, 1996, **79**(12), 3329.
19 S. Preusser, U. Stimming and K. Wippermann, *Electrochim. Acta*, 1996, **39**(8/9), 1273.
20 L. Gal-Or, I. Silberman and R. J. Chaim, *J. Electrochem. Soc.*, 1991, **138**(7), 1939.
21 M. D. Porter, T. B. Bright, D. L. Allara and C. E. D. Chidsey, *J. Am. Chem. Soc.*, 1987, **109**, 3559.
22 K. Bandyopadhyay, K. Vijayamohanan, G. S. Shekhawat and R. P. Gupta, *J. Electroanal. Chem.*, 1998, **447**, 11.
23 E. Sabatani, I. Rubinstein, R. Maoz and J. Sajiv, *J. Electroanal. Chem.*, 1987, **219**(12), 365.
24 C. D. Bain, H. A. Biebucky and G. M. Whitesides, *Langmiur*, 1989, **5**, 723.
25 A. Milchev, *Contemporary Physics*, 1991, **32**(5), 321.
26 C.-J. Zhong and M. D. Porter, *J. Electroanal. Chem.*, 1997, **425**, 147.
27 E. Sabatani, J. Cohen-Boulakia, M. Bruening and I. Rubenstein, *Langmuir*, 1993, **9**, 2974.
28 M. Sluyters-Rehback and J. H. Sluyters, *Electroanalytical Chemistry*, ed. A. J. Bard, Dekker, New York, 1970, vol. 4.
29 H. O. Finklea, D. A. Sinder, J. Fedyk, E. Sabatani, Y. Gaini and I. Rubinstein, *Langmuir*, 1993, **9**, 3660.
30 K. Tokuda, T. Gueshi and H. Matsuda, *J. Electroanal. Chem.*, 1979, **102**, 41.
31 Impedance data were analysed with commercially available software (named equivalent circuit) written by B. A. Boukamp (University of Twente).
32 Approximate coverage (θ) of the dithiols on gold electrode can be measured using charge transfer resistance of bare (R_{ct}) and monolayer coated (R_{ct}') gold electrode by using the relation $\theta = 1-[R_{ct}/R_{ct}']$. R_{ct}s are calculated from the impedance plane plot at higher frequency in the presence of both the oxidized and reduced species present in the solution. Charge transfer resistance is expected to increase at monolayer covered electrode due to inhibition of electron transfer compared to bare electrode.
33 D. G. Castner, K. Hinds and D. W. Grainger, *Langmuir*, 1996, **12**, 5083.
34 Z. Mekhalif, J. Riga, J. J. Pireaux and J. Delhalle, *Langmuir*, 1997, **13**, 2285.
35 A. Henglein, *Top. Curr. Chem.*, 1988, **143**, 113.
36 J. Liu, X. Feng, G. E. Fryxell, Q. Wang and Y. Kim, *Adv. Mater.*, 1998, **10**, 161.
37 C. T. Kresge, M. E. Leonowicz, W. T. Roth, J. C. Vartuli and J. S. Beck, *Nature*, 1992, **359**, 710.
38 P. B. Messersmith and S. I. Stupp, *Chem. Mater.*, 1995, **7**, 454.